

Advanced Practical Course F1

Experiment K1

Quantum Hall Effect

Contents

1	Classical treatment of electrons in electric and magnetic fields (Drude model)	3
1.1	The classical Hall-effect for low magnetic fields	4
1.2	The classical Hall-effect for high magnetic fields	5
1.3	Motion of an electron in an ‘antidot’ lattice	7
2	The semiconductor device for observing the QHE	8
2.1	Formation of a two-dimensional electron gas	9
3	Energy quantization in a magnetic field	12
3.1	Landau levels	12
3.2	Strong localization through disorder	14
3.3	Thermal scattering at the Fermi-edge	15
3.4	Model of edge channels	16
3.5	Shubnikov-de Haas Oscillations	20
3.6	Quantum Hall Effect	21
4	The Experiment	23
4.1	Experimental setup and sample properties	23
4.2	Measurement procedure	25
4.3	Practical report	27
5	Further Reading	29

Over the past four decades, electronic semiconductor technology has experienced a rapid development. For example, the number of transistors on a microchip has approximately doubled every 2 years; an exponential growth rate known as ‘Moore’s Law’. In the early 60’s there were only a few transistors that could be placed on one single chip, however modern CPUs (as at 2014) have $\sim 10^9$! This is achieved using (almost exclusively) silicon CMOSFETs. These “complementary metal-oxide-semiconductor field-effect-transistors” have minimal energy dissipation, and therefore it is possible to have high packing densities. The behaviour of these transistors is determined by a two-dimensional electron gas (2DEG), which forms at the interface between the semiconductor and the oxide layer (an insulating layer between the metallic gate and the semiconductor). In this case the charge carrier density in the 2DEG can be controlled by varying the gate voltage.

In the year 1980, the Quantum Hall Effect (QHE) was discovered by Klaus von Klitzing, who was awarded the Nobel Prize for this work just five years later. He investigated the Hall-voltage of a 2DEG of a Silicon-MOSFET as a function of the charge carrier density at low temperatures and with large magnetic fields applied. Rather than a continuous increase of the Hall voltage with decreasing carrier density or increasing magnetic field, as would be expected from the classical Hall effect, he found that the Hall resistance increases in discrete steps. The precision with which the Quantum Hall effect can be observed in such a MOSFET is noteworthy, since the scattering of the charge carriers in the 2DEG is relatively large. Since this initial work, further research has shown that 2DEGs at interfaces in semiconductor heterostructures are of paramount importance, because particularly high charge carrier mobilities can be achieved due to a low defect densities at the interfaces.

The aim of this practical is to observe both the quantization of the Hall resistance, and the Shubnikov-de Haas oscillations of the longitudinal resistance in a two-dimensional electron system of a GaAs/AlGaAs-Heterostructure. Both effects will be measured in two different semiconductor interfaces - one conventional structure, and another that has a pattern of holes (antidot lattice) etched in the vicinity of the 2DEG. Additionally, the charge carrier density in the 2DEG will be varied with the aid of a surface electrode mounted on the sample. The probe is cooled using liquid helium, which has a temperature of 4.2 K at atmospheric pressure. High magnetic fields up to 5 Tesla will be applied to the sample using a superconducting coil, which is cooled through direct contact with the liquid helium.

1 Classical treatment of electrons in electric and magnetic fields (Drude model)

Consider a current \vec{I} flowing in a semiconductor, perpendicular to an external magnetic field \vec{B} . In a suitable geometry, there will be a voltage established that is perpendicular to both the current and the magnetic field; the so-called ‘Hall voltage’. In this section we will review the classical Hall effect in the framework of the Drude model. In understanding the quantum Hall effect, it is instructive to distinguish between the case of strong scattering, and the situation where the charge carrier movement is nearly ballistic. In the solid state both electrons and holes can facilitate the movement of charge, however in the sample used in this practical, electrons are the charge carriers.

The trajectory of an electron under the influence of electric and magnetic fields is described as the solution of the motion equation

$$\vec{F} = m_e \dot{\vec{v}} = -e(\vec{E} + \vec{v} \times \vec{B}) . \quad (1)$$

where e is the charge of an electron, m_e its mass, and \vec{v} its velocity. Assuming the electric and magnetic fields are perpendicular to each other (i.e. $\vec{E} = E_x \hat{x}$ and $\vec{B} = B_z \hat{z}$), the solution to this equation is so-called ‘cyclotron motion’; a superposition of a circular orbit with cyclotron frequency $\omega_c = eB/m$, and a linear motion with velocity E/B . The uniform component of the motion is perpendicular to *both* applied fields \vec{E} and \vec{B} ! The electron therefore moves in a spiral trajectory along the equipotential lines.

If we now consider the electron to be inside a crystal rather than completely free, then most of the effects of the crystal-field potential (the periodic potential of the crystal lattice) can be accounted for simply by modifying the mass of the electron: The free electron mass m_e in Equation (1) is replaced with an *effective* mass m . As an example, in GaAs, the effective mass of an electron is $m \simeq 0.07 m_e$. In practice, the crystalline lattice is not perfect, and the scattering of the electron from defects, lattice vibrations (i.e. phonons) and other electrons must be taken into account. This can be included phenomenologically by introducing an impulse-relaxation time τ , which is a measure of the time in which the charge carrier will be scattered. With the addition of this damping term, the equation of motion becomes;

$$\vec{F} = \left. \frac{d\vec{p}}{dt} \right|_{\text{Scattering}} + \left. \frac{d\vec{p}}{dt} \right|_{\text{Fields}} = \frac{m\vec{v}}{\tau} - e(\vec{E} + \vec{v} \times \vec{B}).$$

This equation is easily solved in the steady-state (where $F = 0$). With a magnetic field assumed to be along the \hat{z} -direction ($\vec{B} = B\vec{e}_z$), perpendicular to the electric field, the solution can be written in matrix form as;

$$\begin{pmatrix} E_x \\ E_y \end{pmatrix} = \begin{pmatrix} m/e\tau & -B \\ +B & m/e\tau \end{pmatrix} \begin{pmatrix} v_x \\ v_y \end{pmatrix} .$$

With the chosen orientation of the \vec{E} and \vec{B} fields, the electrons experience no motion in the \hat{z} -direction, and therefore this two-dimensional solution provides a complete description. This equation can be re-written in the form of Ohm's law $\vec{E} = \hat{\rho} \vec{j}$ by substituting for the cyclotron frequency $\omega_c = eB/m$, the specific conductivity $\sigma_0 = e^2 n_e \tau / m$, and the current density $\vec{j} = e \langle \vec{v} \rangle n_e$:

$$\begin{pmatrix} E_x \\ E_y \end{pmatrix} = \sigma_0^{-1} \begin{pmatrix} 1 & -\omega_c \tau \\ \omega_c \tau & 1 \end{pmatrix} \begin{pmatrix} j_x \\ j_y \end{pmatrix}, \quad (2)$$

Where n_e is the charge-carrier density, and $\langle \vec{v} \rangle$ indicates the expectation value of the electron velocity. Due to the presence of the magnetic field, the ohmic resistance is now anisotropic, and is therefore represented as a tensor;

$$\hat{\rho} = \sigma_0^{-1} \begin{pmatrix} 1 & -\omega_c \tau \\ \omega_c \tau & 1 \end{pmatrix} \quad (3)$$

If there is no magnetic field applied, then the off-diagonal terms disappear, and Equation (2) reduces to the well known form of Ohm's Law $U = R \cdot I$. The resistance along the same direction as the electric field (the longitudinal resistance) is independent of the magnetic field, and $\rho_{xx} = \rho_{yy} = \sigma_0^{-1}$. The resistance perpendicular to the electric field direction (transverse resistance) is $\rho_{yx} = -\rho_{xy} = \sigma_0^{-1} \omega_c \tau = B / e n_e$, and is proportional to the magnetic field strength.

1.1 The classical Hall-effect for low magnetic fields

A typical experimental arrangement is shown schematically in Figure 1. Experimentally,

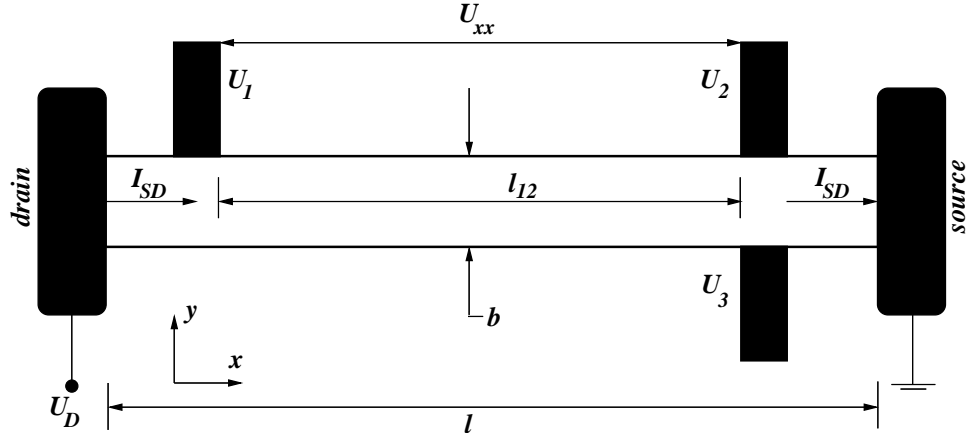


Figure 1: Principal of the measurement of a Hall-voltage $U_{yx} = U_2 - U_3$ and the longitudinal voltage $U_{xx} = U_1 - U_2$.

the resistivity tensor defined in Equation (3) is determined by applying a constant current longitudinally (\hat{x} -direction) through a rectangular sample, and measuring the voltage drop across the longitudinal ($U_{xx} = U_1 - U_2$) and transverse

($U_{yx} \equiv U_H = U_2 - U_3$) directions as a function of the applied magnetic field $\vec{B} = B\vec{e}_z$.

In the arrangement sketched in Fig.1, the voltages are related to the electric fields as $U_{xx} = E_x l_{12}$ and $U_{yx} = E_y b$. Assuming a relatively small magnetic field strength (i.e. $\omega_c \tau \ll 1$), then $E_y \ll E_x$, and in the steady state the current is uniformly distributed in the \hat{x} -direction with $j_x = I/b$ and $j_y = 0$. Physically the condition $\omega_c \tau \ll 1$ implies that the scattering of the electrons is so strong, that the momentum distribution corresponds to a thermodynamic equilibrium superimposed on a constant drift in one direction. Therefore, a ‘drift velocity’ can be defined for the electrons as $v_d = \langle v \rangle$. In this case, the relationship between the components of the resistance tensor and the measured voltages are;

$$\rho_{xx} = \frac{U_{xx}}{I} \frac{b}{l_{12}} \quad \text{und} \quad \rho_{yx} = \frac{U_{yx}}{I}.$$

Using the relation $\rho_{yx} = B/en_e$, the charge-carrier density in the Hall-probe can be obtained from a measurement of U_{yx} at small magnetic fields as

$$n_e = \left(e \frac{d\rho_{yx}}{dB} \right)^{-1} = \frac{I/e}{dU_{yx}/dB}$$

Also, in this regime of low magnetic field, the mobility of the electrons can be determined. This is defined as the absolute value of the ratio of the drift velocity to the electric field:

$$\mu_e = \left| \frac{v_d}{E_x} \right| = \frac{\sigma_0}{en_e}.$$

1.2 The classical Hall-effect for high magnetic fields

In the previous section the case where $\omega_c \tau \ll 1$ was considered. Here we will consider the opposite limit, where a very large magnetic field is applied, i.e. $\omega_c \tau \gg 1$. The resistivity tensor (3) can be converted through matrix inversion to a conductivity tensor $\hat{\sigma}$ defined through $\vec{j} = \hat{\sigma} \vec{E}$;

$$\hat{\sigma} = \sigma_0 \begin{pmatrix} \frac{1}{1+\omega_c^2 \tau^2} & \frac{\omega_c \tau}{1+\omega_c^2 \tau^2} \\ -\frac{\omega_c \tau}{1+\omega_c^2 \tau^2} & \frac{1}{1+\omega_c^2 \tau^2} \end{pmatrix}. \quad (4)$$

When no magnetic field is applied, the off-diagonal elements of the conductivity tensor are zero, as is also the case for the resistivity tensor. Equation (4) then is simply Ohm’s law in its scalar form, and the current flows in the direction of the applied electric field. In the longitudinal direction, at low magnetic field, Ohm’s law to first order implies $\sigma_{xx} = \rho_{xx}^{-1} = \sigma_0$. However in the limit of high magnetic fields ($\omega_c \tau \gg 1$), the result is somewhat surprising;

$$\sigma_{xx} \longrightarrow \frac{\sigma_0}{(\omega_c \tau)^2} = \frac{(en)^2}{B} \frac{1}{\sigma_0} \propto \rho_{xx} !$$

This dependence seems paradoxical: The conductivity σ_{xx} in the longitudinal direction is proportional to the resistivity ρ_{xx} . This indicates that in the presence of a strong magnetic field, Ohm's law of the form $U = R \cdot I$ is no longer valid. The off-diagonal elements for large applied magnetic fields are $-\sigma_{xy} = \rho_{yx}^{-1} (= en_e/B)$, and for small magnetic fields reduce to $-\sigma_{xy} = \sigma_0^2 \rho_{yx}$.

These results can be understood pictorially, by considering the equipotential lines in the sample. The upper section of figure 2 depicts the equipotential lines for the case of a negligibly small magnetic field. The current density is evenly

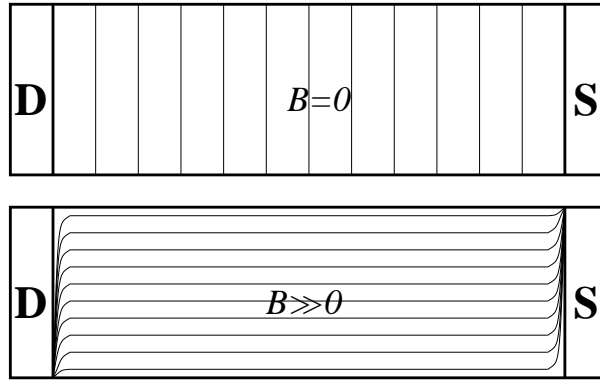


Figure 2: Schematic representation of the equipotential lines in a two-dimensional Hall-probe without magnetic field (above) and in the presence of a large magnetic field perpendicular to the probe plane (below).

distributed in the sample, and $j_y = 0$. If a strong magnetic field perpendicular to the plane of the sample is applied ($\omega_c \tau \gg 1$) simultaneously with an electric field in the longitudinal direction, then by solving the equations of motion (2), it can be seen that $j_y = 0$ no longer applies for the whole sample.

The electrons are driven primarily by the strong magnetic field, and only weakly by the electric field, in the source-drain direction. A large Hall voltage results as a consequence of the sample's finite width, as shown by the equipotential lines sketched in the lower part of figure 2. This picture shows how in strong magnetic fields, the Hall voltage is identical to the source-drain voltage, i.e. $U_{SD} \equiv U_x = U_y \equiv U_H$. The equipotential lines indicate that the upper right corner of the sample is at the same potential as the drain contact, and the lower left corner is at the same potential as the source contact. For a sample of length l and width b , we have $E_y/E_x = l/b$. This implies that for an elongated sample with $l \gg b$, the electric field in the transverse direction can be much larger than the field due to the source-drain voltage in the longitudinal direction. In the periods between scattering (recall $\omega_c \tau \gg 1$), the electrons move in a spiral-like trajectory along the lines of equal potential. Almost all of the voltage drop in the longitudinal direction occurs very close to the source and drain contacts at the so-called 'hot spots', where the equipotential lines are closest together. It has been observed experimentally that a

current-carrying sample will be notably heated in these particular locations.

Note that due to the inhomogeneous distribution of the electric field in the sample, the local longitudinal resistance ρ_{xx} can not be measured using the source-drain contacts. This requires a four-point measurement, where instead of measuring U_{SD} , the voltage U_{xx} is measured (see Fig. 1) in the presence of a constant source-drain current. In this measurement setup, the leads for the voltage measurement are current-free, which means that their resistance is not included in the measurement. Specifically, in such a four-point measurement, the voltage drop across the ‘hot spots’ will not be included ($U_{SD} > U_{xx}$).

1.3 Motion of an electron in an ‘antidot’ lattice

In the following, the discussion will be limited to the case where $\omega_c \tau \gg 1$, meaning that the scattering of the electrons will be neglected. The general solution of the equation of motion (Eqn. 1), with the boundary condition $E_y/E_x = l/b$, is cyclotron motion of the form;

$$\vec{v} = -\frac{e}{m\omega_c} \begin{pmatrix} \frac{l}{b} E_x \\ -E_x \end{pmatrix} + v_0 \begin{pmatrix} \cos \omega_c t \\ \sin \omega_c t \end{pmatrix} \quad (5)$$

With $l \gg b$, the y -component of the linear-motion can be neglected. The orbital radius (cyclotron radius) of the circular component of the electron trajectory is determined by the magnetic field. For an electron with a Fermi-velocity v_F , this radius is given by;

$$R_c = \frac{v_F}{\omega_c} = \frac{m}{eB} \frac{\hbar}{m} \sqrt{2\pi n_e} = \frac{\hbar}{eB} \sqrt{2\pi n_e} .$$

It is possible to impose an artificial periodic lattice of scattering centres on a two-dimensional Hall-probe - a so-called ‘antidot’ lattice. The term ‘antidot’ implies a non-conducting region, small in extent, in the otherwise conducting environment (i.e. the opposite to the case of an isolated electron island which has come to be known as a ‘quantum dot’). The transport properties of a Hall-probe are significantly affected by the antidot scattering centres. Figure 3 depicts some possible electron orbits, for the case where $l \gg b$, in a sample with an antidot lattice. When the orbit diameter is smaller than the spacing of the antidots, then there are so-called ‘runaway trajectories’, and the longitudinal resistance is reduced. At specific values of the magnetic field, the cyclotron radius $R_c(B)$ describes closed orbits, which enclose one or more antidots. These closed paths result in a localization of the electrons in the antidot lattice, and implies an increased resistance in the probe (see also Chapter 3.2). One property to be investigated in this experiment, is how the longitudinal resistance is affected by these antidots as a function of the magnetic field, which is defining the cyclotron radius. It should also be noted that the presence of antidots also affects the potential-energy landscape, which in turn modifies the electron orbits.

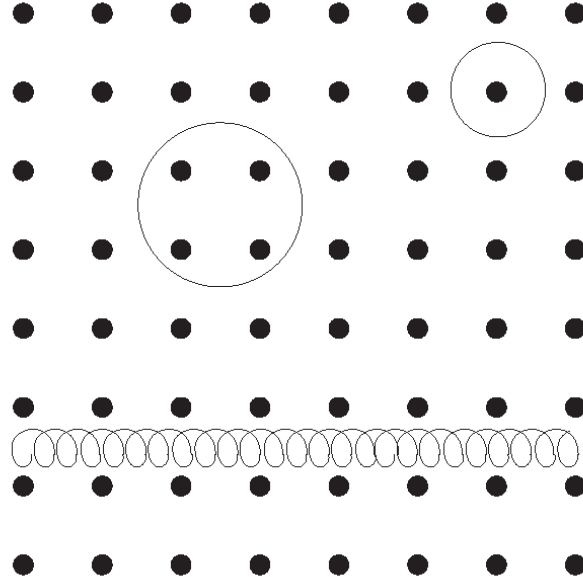


Figure 3: Sketch of electron trajectories in a probe with an antidot lattice for three different magnetic fields.

2 The semiconductor device for observing the QHE

In the last chapter, the physical phenomena introduced could be completely described using a *classical* electrodynamic model. In this chapter we consider the necessary conditions for observing the *quantum* hall effect. Ultimately this requires that the charge carrier density of states resembles that of a fully quantized, i.e. zero-dimensional system.

The motion of the charge carriers can be confined to just two dimensions by careful design of the semiconductor layers and the band structure (discussed in more detail below). Then the charge carrier energies can be further quantized within this 2-D planar ‘electron gas’ through the application of a large magnetic field. To observe this full quantization, the relationship $\omega_c \tau \gg 1$ must be fulfilled. In practice, the magnetic field strength achievable is limited, therefore to satisfy this condition requires a long time between scattering τ , or equivalently a high degree of mobility $\mu = e\tau/m$ for the charge carriers. As an example, such two-dimensional electron or hole systems can form at the semiconductor-oxide border in MOSFETs (see introduction). The scattering processes due to thermal lattice vibrations (phonons) can be minimized to some extent simply by cooling the probe. The charge carrier mobility is then limited by scattering from crystal defects at the interface. In fact, the oxide layer in MOSFETs is amorphous, which would suggest particularly strong scattering. However, as it turns out, the spatial distribution of the charge carrier’s wavefunction is such that the 2-dimensional system is located

mostly within the semiconductor, and is separated from the interface. Therefore the diffusion effect of scattering from defects is significantly reduced.

In this experiment, a semiconductor-heterostructure with a two-dimensional electron gas (2DEG) near the interface between GaAs and n -doped AlGaAs will be used. The advantage of such structures as compared to MOSFETs is that larger mobilities can be achieved. This is primarily due to the growth techniques that allow atomic-layer precision, and thus a high quality crystalline structure, combined with the aforementioned low overlap between the 2DEG and the interface. The following section describes how such a two-dimensional electron gas can form.

2.1 Formation of a two-dimensional electron gas

In an ordinary semiconductor, the conduction electrons are free to move within the volume in all three spatial dimensions. The electron motion is restricted only by scattering within the volume, and by the high potential at the material edge. The electrons in such a material can be modelled as a thermodynamic three-dimensional electron gas. When the movement of the electrons is restricted in one spatial direction, then they are free to move only within a plane. Such a system is often abbreviated as a 2DEG (two-dimensional electron gas). Fig. 4 depicts the interface region between GaAs and AlGaAs in a GaAs/AlGaAs-Heterostructure. With no external voltage applied, and without any doping, the Fermi energy E_F in a continuous sample is directly in the middle of the bandgap, as depicted in Fig. 4(b). Therefore, at temperature $T = 0$ when there are no moving charges, there is a step-like change in the band-edge energies at the interface between the two materials.

However, the band-edge structure across the interface changes significantly if there are additional charge carriers introduced through doping. Such a case is shown in Fig. 4(c), in which the AlGaAs is n -doped. It is assumed that the Donor atoms are distributed homogeneously throughout the AlGaAs crystal. Due to the difference in chemical-potential of the two materials, the donor-electrons re-arrange themselves in the vicinity of the GaAs, and the band-edge bends correspondingly in the interface region. Key features to note from the self-consistent solution of this system are that the AlGaAs has a larger bandgap compared to GaAs, and that the Fermi-energy in the AlGaAs lies just below the conduction band edge due to the n -doping. With a specifically chosen dopant concentration, the conduction band on the GaAs side of the interface has a very narrow triangular potential well, whose minimum lies below the Fermi level. The precise location and contour of the potential-well determines the extent of the electron wave-functions and their interactions. It is important that the overlap between the electron wavefunctions in the 2DEG and the interface layer is minimized. Thus, the scattering of charge carriers within the 2DEG caused by surface defects or donor-atom centres in the AlGaAs are minimized (as discussed earlier in the case of MOSFETs).

Due to the strong spatial confinement in this triangular potential, the solution of the Schrödinger equation indicates that the energy-spectrum becomes discrete the z -direction, whereas the energy values related to the transverse momentum (for

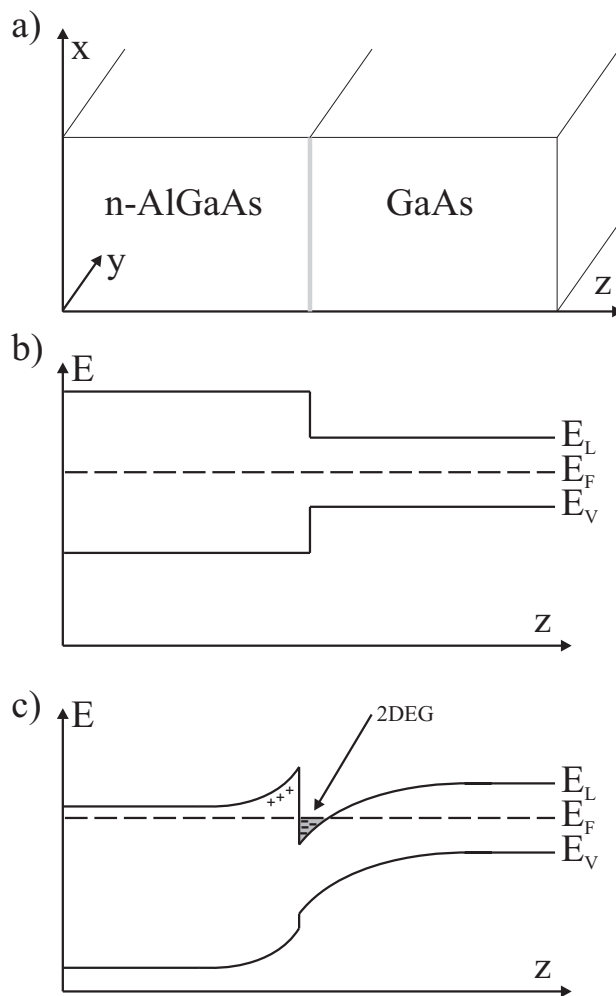


Figure 4: Deformation of the band-edge in a heterostructure.

sufficiently large lateral extent of the sample) remains continuous. The spectrum of electron states are grouped according to their momentum in the z -direction into so-called subbands. The dispersion relation of the 2DEG is given by

$$E = E_c + \varepsilon_s + \frac{\hbar^2}{2m} (k_x^2 + k_y^2) . \quad (6)$$

where E_c is the energy of the conduction band edge at the minimum of the triangular potential well. The subband energy ε_s takes on discrete values indicative of the quantized motion in the z -direction. At the low temperatures used in this experiment, only the lowest energy subband, with energy ε_0 , is populated. The last term in the equation describes the kinetic energy associated with the electron's motion in the xy plane.

The next task is to determine the density of states of the electrons in the 2DEG.

This is achieved by counting the number of states in the k_x - k_y momentum space that exist within a circle with radius k . With periodic boundary conditions, the allowed quantized values for k_x and k_y are

$$k_x = n_x(2\pi/l) \quad \text{and} \quad k_y = n_y(2\pi/b)$$

where l and b are the dimensions of the sample in x and y directions respectively, and n_x and n_y are integers. We can determine the ‘area’ in momentum-space corresponding to a single (k_x, k_y) state as;

$$\frac{2\pi}{l} \cdot \frac{2\pi}{b} = \frac{4\pi^2}{S} .$$

Here $S = l \times b$ is the area of the sample in real space. Including spin, (2 states per $\frac{4\pi^2}{S}$), then we have the number of states $Z(E)$ that are contained within a circle of area πk^2 in k -space (for $E > E_c + \varepsilon_0 \equiv E_0$) as

$$Z(E) = 2 \frac{\pi k^2}{4\pi^2/S} = S \frac{k^2}{2\pi} = \frac{mS}{\pi\hbar^2} (E - E_0) ,$$

where the last equality follows from Eqn.6. Finally, the density of states in a 2DEG takes the form

$$N(E) = \frac{1}{S} \frac{d}{dE} Z(E) = \frac{m}{\pi\hbar^2} \theta(E - E_0) \quad (7)$$

The Theta-Funktion has the following meaning;

$$\theta(E - E_0) = \begin{cases} 0 & \text{für } E < E_0 \\ 1 & \text{für } E > E_0 \end{cases} .$$

Physically, this function means that there are no states that can exist with $E < E_0$. An important feature of this two-dimensional system is that for $E > E_0$, the density of states for the electrons is independent of the energy.

3 Energy quantization in a magnetic field

In the previous chapter, we saw that the spatial restriction of the electron system in one dimension led to a quantization of the energy spectrum associated with this dimension. Further quantization of the energy spectrum can be induced through the application of a large magnetic field. Physically the magnetic field quantizes the angular momentum, where any motion perpendicular to the magnetic field can only occur within certain cyclotron paths having radii $R_c = v/\omega_c$. If the magnetic field is applied such that it is perpendicularly oriented with respect to the 2DEG, then the electron motion becomes restricted in all three spatial dimensions. However, in order to observe this fully quantized energy spectra, the charge carriers cannot be scattered out of their cyclotron paths, i.e. we must satisfy the condition $\omega_c\tau \gg 1$. In addition to this, a second condition for observing the discrete energy spectra is that the energy-spacing between the allowed energy levels must be greater than the thermal energy of the electrons (i.e. the ‘sharpness’ of the Fermi edge).

3.1 Landau levels

To investigate the energy quantization in a magnetic field, we begin with the Schrödinger equation for a two dimensional electron system

$$\hat{H}\Phi = \left[-\frac{\hbar^2}{2m} \left(\vec{\nabla} - \frac{e\vec{A}}{i\hbar} \right)^2 \right] \Phi = E\Phi . \quad (8)$$

The magnetic vector-potential \vec{A} must be chosen such that the condition $\vec{B} = \vec{\nabla} \times \vec{A}$ is fulfilled. With a \vec{B} -field applied in the z -direction (perpendicular to the 2DEG), and in the Landau-gauge the vector potential becomes $\vec{A} = (0, Bx, 0)$. Because the symmetry in the z -direction is characterized by the magnetic field and 2DEG, the wave function can be found using a separation-of-variables approach.

$$\Phi(x, y, z) = \zeta(x, y)\xi(z)$$

The eigenvalues for energy of $\xi(z)$ are the subband energies ε_s introduced earlier (Eqn.6). The remaining task is to solve the Schrödinger equation (8) for the transverse component of the wavefunction $\zeta(x, y)$.

$$-\frac{\hbar^2}{2m} \left[\frac{\partial^2}{\partial x^2} - \frac{eBx}{i\hbar} \frac{\partial}{\partial y} + \frac{\partial^2}{\partial y^2} - \left(\frac{eBx}{\hbar} \right)^2 \right] \zeta(x, y) = E\zeta(x, y) .$$

A common approach, related with choosing the Landau-gauge previously, is to assume the wavefunction takes the form

$$\zeta(x, y) = e^{-ik_y y} \psi(x) ,$$

such that the Schrödinger equation then reduces to

$$-\frac{\hbar^2}{2m} \left[\frac{\partial}{\partial x^2} + \frac{eBk_y x}{\hbar} - k_y^2 - \left(\frac{eBx}{\hbar} \right)^2 \right] \psi(x) = E\psi(x) .$$

Making the substitutions for the cyclotron frequency $\omega_c = eB/m$, and also letting $x_0 \equiv \hbar k_y/eB$, we finally arrive at

$$-\frac{\hbar^2}{2m} \frac{\partial^2 \psi}{\partial x^2} + \frac{m}{2} \omega_c^2 (x - x_0)^2 \psi(x) = E\psi(x) .$$

This is the differential equation corresponding to a one-dimensional harmonic oscillator. The solutions to this are given by the ‘Hermite’ polynomials. The eigenvalues of the energy correspond to the so-called *Landau-levels*

$$\varepsilon_n = \hbar\omega_c \left(n + \frac{1}{2} \right) , \quad (9)$$

where $\frac{1}{2}\hbar\omega_c$ is the zero-point energy, and $n = 0, 1, 2, \dots$ is the quantum number of the Landau-level. In equation (9), the Zeeman-splitting due to the magnetic field has not been included. Fig. 5 depicts the spin-split Landau levels. In this

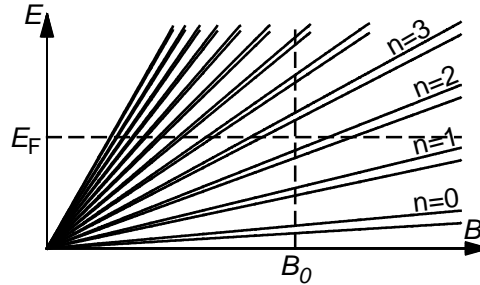


Figure 5: Energy of the first 12 spin-split Landau-levels as a function of the magnetic field. The magnitude of the Zeeman-splitting is strongly exaggerated for clarity. When the magnetic field is at B_0 , only the lowest three Landau-levels will be populated.

example, the Fermi energy E_F at the magnetic field B_0 lies between the third and fourth Landau-level, such that at field (and at low temperature) only the lowest three Landau-levels having $n = 0, n = 1$ and $n = 2$ will be occupied.

Taking the conduction-band energy E_c as the zero-point energy reference, and considering that at low temperature only the lowest subband is occupied, then the Landau-quantization with magnetic field (Eqn.6) can be simplified as

$$E_n = \varepsilon_0 + \varepsilon_n = \varepsilon_0 + \hbar\omega_c \left(n + \frac{1}{2} \right) . \quad (10)$$

In the presence of a magnetic field, the density of states (for $E > E_0$) is no longer constant, but becomes instead a series of δ -functions separated by energies $\hbar\omega_c$ i.e. the Landau-levels. The states which were previously existing within the energy intervals $\hbar\omega_c$, are now distributed to the distinct Landau-levels. For instance, the previously finite density of states value at the Fermi-energy is now zero, unless the condition $E_n = E_F$ is met. From the density of states (Eqn.7) it follows that the number of states in each Landau-level per unit area is;

$$N = \hbar\omega_c \frac{m}{\pi\hbar^2} = \frac{2eB}{h} . \quad (11)$$

This is assuming that the Zeeman-splitting is so small that it is not resolved, and therefore effectively the spin-separation is negligible.

All of the $n_e l b$ free electrons must be distributed between the available Landau levels. Therefore, Eqn.11 can be used to determine the number of occupied Landau-levels as

$$\frac{n_e}{N} = \frac{n_e h}{2eB} .$$

For example, if this expression takes a value $n_e/N = 5.2$, then this means that five Landau-levels are filled, with some partial occupation of the sixth. In this instance, the sixth Landau-level lies the closest to the Fermi energy E_F . Accounting also for the two-fold spin-degeneracy of each Landau-level which may be lifted in large magnetic fields due to the Zeeman effect, we arrive at the so-called fill factor ν , defined as;

$$\nu = \frac{n_e h}{eB} . \quad (12)$$

In the above example, the fill factor would be therefore $\nu = 10.4$. If we continuously increase the magnetic field with the carrier density remaining constant, then the number of states per Landau-level will increase, and the fill factor will decrease.

The variation of the density of states with respect to the Fermi-energy as a function of magnetic field has interesting consequences for the resistance tensor and the charge-transport properties of a Hall-probe in the quantum mechanical regime. Of particular interest in this practical, is the quantum Hall effect and the Shubnikov-de-Haas oscillations, which will both be measured.

3.2 Strong localization through disorder

Figure 6 is a sketch of the density of states of a 2DEG for a finite magnetic field with spin-splitting included. In the case shown, there are two Landau-levels with energies below the Fermi energy, and therefore only these two levels will be occupied at low temperatures. In reality, even at extremely low temperatures the Landau-levels are not δ functions, but are significantly broadened. This is due to the effect of disorder within the crystal lattice. A random distribution of defects will cause a spatial perturbation of the crystal field potential through their electric and elastic moments. The crystal field potential becomes like a mountain landscape

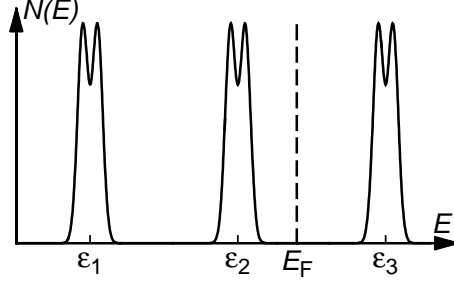


Figure 6: Density of states for the charge carriers in a 2DEG with a large magnetic field applied. The energy separation between the spin-split Landau-levels is $\hbar\omega_c$. In the case sketched here, there are two Landau-levels with energies below the Fermi energy. Therefore, at sufficiently low temperatures, only these two levels will be occupied.

with peaks and valleys, and this effectively causes a broadening of the energy distribution within a Landau level in the 2DEG.

The solution of the equation of motion (Eqn.1) for free electrons in a magnetic field gives cyclotron paths of the form given in Eqn.5. When the random spatial modulation of the crystal field which occurs in a real solid are accounted for, the motion is no longer occurring exactly on cyclotron paths. Rather, the charge carriers move along equipotential lines which are compatible with the cyclotron radius it would have in an ideal crystal. In general, these closed paths are either along the edge of a potential valley, or orbiting a peak. This leads to a strong localization of charge carriers in the fully occupied Landau levels. This localization can however be hindered through inelastic scattering.

3.3 Thermal scattering at the Fermi-edge

The particular properties of Fermions are paramount in any discussion of the scattering of electrons in solid-state bodies, and therefore we will briefly revise some key points here. At temperature $T = 0$, all states having energy $E < E_F$ will be filled with charge carriers, while all remaining states outside this so-called "Fermi sphere" will be unoccupied. If the Fermi energy is overlapping with one of the Landau levels, then the states within this Landau level will be partially occupied. At finite temperatures, the charge carriers can be scattered due to thermal lattice vibrations. The amount of thermal energy available is $\sim k_B T$, therefore charges can also occupy states where $|E - E_F| \lesssim k_B T$. These charge carriers are scattered outside of the Fermi sphere. However, even at room temperature for real solids typically $k_B T \ll E_F$, then only a small fraction of the total charge carriers are contributing to this 'smearing out' of the Fermi surface. This is because for the majority of electrons, which have lower energies $|E - E_F| \gg k_B T$, there are

no available empty states within $\delta E \sim k_B T$ for them to scatter into. Therefore, in sufficiently large magnetic fields where $\hbar\omega_c \gg k_B T$, then the electrons in the fully-occupied Landau levels cannot be scattered.

At large temperatures (or equivalently small magnetic fields) where $\hbar\omega_c \ll k_B T$, then the thermal broadening of the Fermi edge is so large that the Landau levels are not energetically resolvable, and the density of states around the Fermi energy is only weakly modified compared to the 2DEG case. In this scenario the 'soft' Fermi edge overlaps with many different Landau levels. Therefore, the previously mentioned situation where there are many charge carriers that cannot be scattered (i.e. with Landau quantization) only becomes observable at sufficiently low temperatures (or large magnetic fields) such that $\hbar\omega_c \gg k_B T$.

3.4 Model of edge channels

After the discussion in the previous two sections, we may develop the expectation that with $\hbar\omega_c \gg k_B T$, when there is no Landau level overlapping with the Fermi edge, then localization of the electron motion occurs and the resistance is maximized. Surprisingly, experimental observations are exactly the opposite: The longitudinal resistance of a Hall-probe can, with sufficiently large magnetic field, actually disappear! The explanation of this somewhat astonishing result is found when considering what happens in the transverse direction within the 2D plane, and the finite size of the sample.

In the following we present a mostly classical argumentation will be presented to give some insight into how this occurs. At the edge of the sample, the electrons would need to overcome the work function to leave the solid, which is a very high potential barrier. Not only is the energy required large, but the gradient is very steep. On this potential energy edge, the previously discussed 'mountains and valleys' of the crystal field disorder are rendered negligible. Therefore, the charge carriers right on the edge of the sample will not be restricted to localized orbitals. Instead, they will bounce off this potential as if it were a smooth mirror, and will travel in this way along the edge of the sample. This edge-reflection effect gives rise to so-called 'edge channels', which conduct electrons from one end of the sample to the other. Fig. 7 illustrates the influence of the boundary potential on the localization of the electrons.

To develop this model in a semi-classical approximation, we expand the energy of the Landau-levels in Eqn.10 around the edge potential $U(y)$

$$E(n, y) = \varepsilon_0 + \hbar\omega_c \left(n + \frac{1}{2} \right) + U(y) ,$$

where $U(y)$ is zero in the centre of the sample, and at the edge becomes infinitely large. The energy of the Landau levels therefore will increase sharply at the edge of the sample, and crosses the Fermi energy. This modification of the Landau level energies is shown in Fig.8. Unlike in the interior of the sample, the density of states at the Fermi level will disappear at the sample edge. The number of edge channels

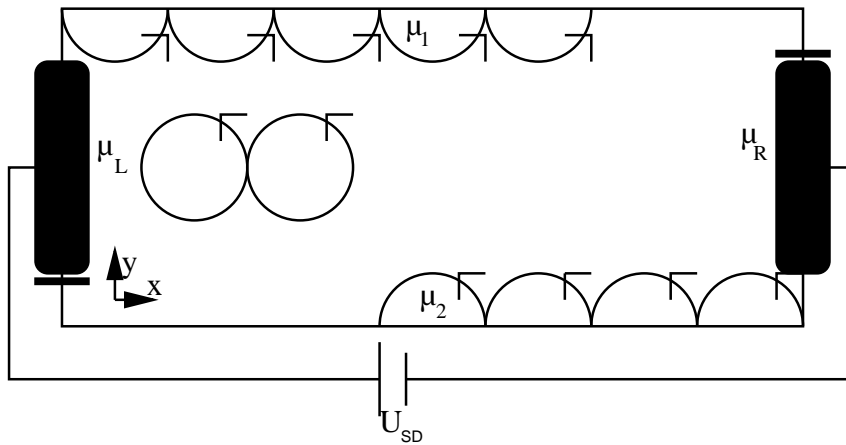


Figure 7: Illustration of the localization of the electrons inside the sample, and the conduction channels along the edge.

therefore is the same as the number of Landau levels in the sample interior having $E < E_F$.

In fact, the edge channels are one-dimensional because of the finite extent of the local electronic wave function and the Pauli principle prohibit a higher electron density. This falls into the category of so called ‘quantum point contacts’. Here we will briefly discuss the quantum mechanical properties of these one-dimensional conductors. A quantum point contact is essentially an additional imposed on a 2DEG. The degree of the constriction can usually be varied by means of an external electric field, and the transition from a two-dimensional electron gas to a one-dimensional ladder - the quantum point contact - can be completed. In a typical experiment, the current through the sample would be measured at a constant applied voltage as a function of the degree of constriction. Fig.9 shows the result of such a measurement of the conductance through a quantum point contact at very low temperature. What can be seen from the figure is that there are levels that are separated by $2e^2/h$, until the conductance eventually disappears completely when the quantum point contact is closed. The conductance quanta e^2/h corresponds precisely to the conductance of a channel which fits exactly one electron. In an analogous measurement without any magnetic field applied, there will be exactly two electrons conductance in each channel due to spin degeneracy. As the channel in a quantum point contact is increasingly constricted, then gradually one by one the number of conductance channels will be reduced, and consequently the conductance ladder with steps of $2e^2/h$ can be observed. This behavior is experimental verification for the quantization of conductance.

The edge channels in a Hall-probe are another example of a one-dimensional channel. This will be the case when there is no Landau level overlapping with the Fermi level $E_n \simeq E_F$, such that in the centre of the probe there is no available energy levels for charge carriers to scatter into, and therefore all charge carriers re-

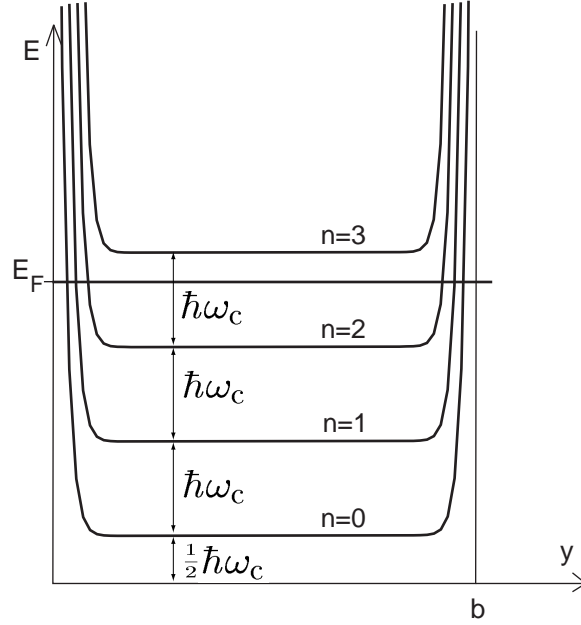


Figure 8: Modification of the Landau levels by the edge-potential (note spin-splitting has been neglected).

main on their localized trajectories, and cannot mediate any net current flow. Each edge channel is associated with a conductance of $2e^2/h$ (spin-degenerate). The spatial separation of the edge channels prevents scattering between the channels. In addition, the electrons that are moving at the Fermi-velocity also have the same momentum as the electrons in adjacent edge channels. According to Lenz's law $-ev_x B = dU(y)/dy$, the electrons in the edge channels at opposite sides of the sample will move in opposite directions. Due to this segregation of the electron current directions, backscattering of the electrons in the edge channels is therefore extremely unlikely. The resulting current through the sample comes from the fact that the Fermi-velocity along the opposite edges of the sample are different because of the Hall voltage. This is depicted in Fig. 10.

From the classical consideration presented earlier, we have already seen from the equipotential lines in Fig.2, that in a strong magnetic field the Hall-voltage is identical to the source-drain voltage ($U_H = U_{SD}$). When the edge channels are solely responsible for charge transport, this result is trivial. Because the edge channel is resistance-free, and therefore there is no voltage drop across the channel, i.e. in Fig. 7 $\mu_1 = \mu_L$ and $\mu_2 = \mu_R$, and the electrons in the upper channel (μ_1) move to the right, and in the lower channel (μ_2) to the left. The entire potential drop occurs only across a very small region, known as the 'hot-spots' (marked with thick lines in Fig. 7). The Hall voltage is then

$$U_H \equiv U_{yx} = -\frac{1}{e}(\mu_1 - \mu_2) = -\frac{1}{e}(\mu_L - \mu_R) = U_{SD} . \quad (13)$$

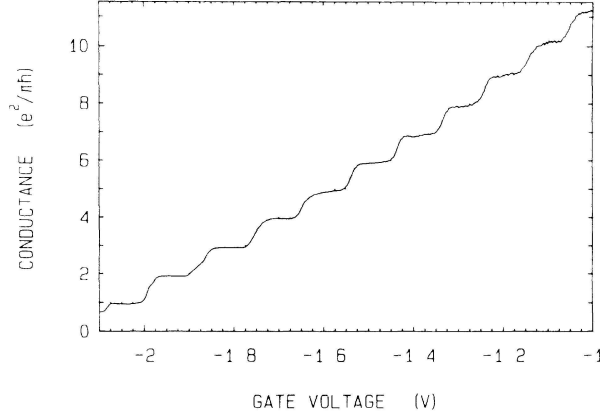


Figure 9: Quantization of the conductance through a quantum point contact. The 1-dimensional channels along the x -axis are opened one by one.

In the following, we will derive the current carried by an edge channel and determine the conductance quanta. In general, the current carried by a charge Q is $I = \langle Q/t \rangle = \langle Q \rangle \langle 1/t \rangle$. If there are β electrons in an edge channel, then $\langle Q \rangle = -e\beta$. In accordance with the Pauli principal, there cannot be more than one electron having the same energy in a particular location. This extent of this region is given by the de-Broglie wavelength $\lambda = 2\pi/k_F = h/mv_F$. Therefore, the number of electrons that fit in the edge channel of length l is given by $\beta = l/\lambda = lm v_F/h$ (or double as many when spin degeneracy is included). To determine the value of $\langle 1/t \rangle = \langle v \rangle /l$, we consider the electron velocity along both the edges;

$$\left\langle \frac{1}{t} \right\rangle = \frac{1}{l} \langle v_{LR} - v_{RL} \rangle$$

The relationship between $eU_{SD} = \mu_L - \mu_R$ and the difference of the edge channel velocities is shown in Fig.10, and is given by

$$\begin{aligned} \mu_L - \mu_R &= \frac{1}{2} m \langle v_{LR}^2 - v_{RL}^2 \rangle \\ &= \frac{1}{2} m \langle (v_{LR} + v_{RL})(v_{LR} - v_{RL}) \rangle \\ &= \frac{1}{2} m 2v_F \langle v_{LR} - v_{RL} \rangle \end{aligned}$$

and with Eqn.(13), the current through an edge channel is then

$$I = \langle Q \rangle \left\langle \frac{1}{t} \right\rangle = -\frac{e}{h} (\mu_L - \mu_R) = \frac{e^2}{h} U_{SD} = \frac{e^2}{h} U_H \quad (14)$$

The transverse resistance per edge channel is therefore

$$R_{xy}^{\text{Kanal}} = \frac{U_H}{I} = \frac{h}{e^2}$$

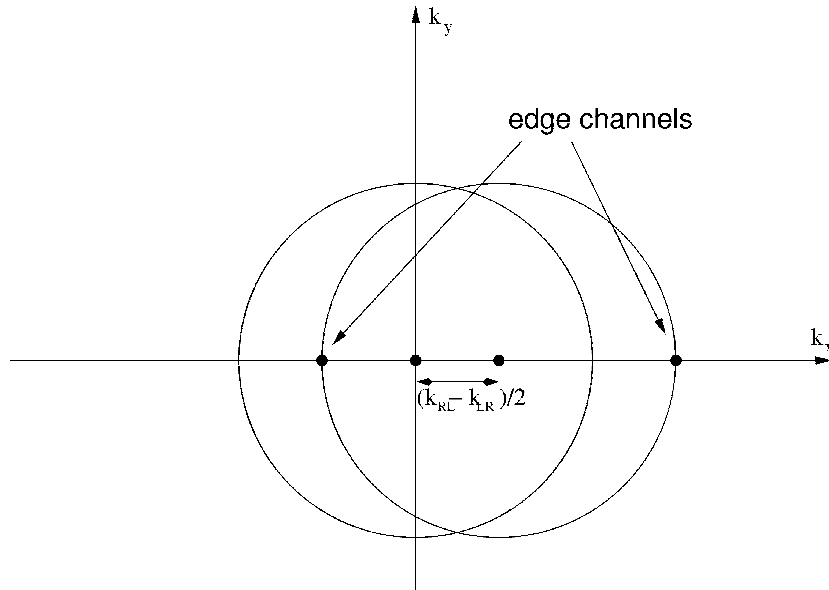


Figure 10: The voltage applied to the sample causes the Fermi-surface to be shifted in the x -direction. The electrons which are moving in the edge channels are at the momentum points where the Fermi circle intersects with the x -axis.

and e^2/h is simply the conductance quanta. With spin degeneracy, the conductance is twice this value, and R_{xy}^{Kanal} is halved.

3.5 Shubnikov-de Haas Oscillations

It is interesting to consider the case when the Fermi energy lies within a Landau-level (which is broadened as a side effect of crystal disorder), i.e. $E_n \simeq E_F$. The Landau level is only partially filled, and due to the finite temperature, the electrons within this level can be thermally scattered, and can consequently move throughout the 2DEG. These electrons are no longer localized, and electrons distributed throughout the entire 2DEG can participate in charge transport. It is important to note that thermal scattering will occur throughout the entire sample, even from the edge channels. In this situation the resistance along the sample is significantly increased. In contrast, the longitudinal resistance disappears when there is no Landau level overlapping with the Fermi-energy, in which case only the edge channels carry current in the x -direction.

This periodic variation in the longitudinal resistance as the magnetic field is varied is known as Shubnikov-de Haas Oscillations. These oscillations are a direct consequence of the magnetic-field induced modulation of the density of states for electrons at the Fermi level. At this point, it should be noted that the course of this magneto-resistance is strongly dependent on the sample geometry. For example, in a sample in which the source and drain electrodes are arranged as concentric circu-

lar discs, there may not be any edge channels. In such a geometry, the Shubnikov-de Haas oscillations would have a resistance minima when the density of states is particularly large at the Fermi-energy. By comparison, the electronic resistance in a Hall-probe behaves somewhat counterintuitively - having a maxima when the density of states at the Fermi energy is large. However this behaviour was also observed in the purely classical Drude-model presented in Chapter 1, where it was shown that for a Hall geometry in the limit of a large magnetic field ($\omega_c\tau \gg 1$), the diagonal components of the resistance and conduction tensors become related as $\rho_{xx} \propto \sigma_{xx}$.

The Shubnikov-de Haas oscillations of the longitudinal resistance of a Hall probe can be used to determine the charge carrier concentration in a 2DEG. The maxima of the longitudinal resistance ρ_{xx} occurs when the fill factor takes half-integer values, since then the density of states at the Fermi-energy is maximal. By measuring the magnetic field strengths B_i and B_{i+1} corresponding to consecutive maxima (or minima) in ρ_{xx} , the carrier concentration can be determined with the use of the fill-factor definition from Eqn.12 as

$$n_e = \frac{e}{h} \frac{1}{(1/B_i) - (1/B_{i+1})}. \quad (15)$$

If the carrier concentration is varied, for instance through the application of an external electric field (perhaps with the help of a capacitor like geometry used in this practicum), then the distance between the ρ_{xx} maxima will change accordingly. Reaching sufficiently large magnetic fields to resolve the Zeeman splitting will not be possible in this practicum, so note that the states are always spin degenerate. With spin degeneracy, such a measurement of the maxima of ρ_{xx} corresponds to integer filling factor values, and the actual carrier concentration differs by a factor of two from that given in Eqn.15.

3.6 Quantum Hall Effect

Experimental measurements of longitudinal and transverse voltage drops across a Hall probe as a magnetic field is ramped show that when the longitudinal resistance ρ_{xx} disappears, there are plateaus in the transverse (Hall) voltage. The Hall resistance corresponding to these plateau regions is given very exactly by the relationship

$$R_H \equiv \rho_{yx} = \frac{R_K}{\nu} \quad \nu = 1, 2, \dots, \quad (16)$$

where ν is the integer portion of the fill factor, as defined in Eqn.12. The Klaus von Klitzing constant R_K is approximately 25.8 k Ω . Obviously the Hall voltage depends also on the magnetic field, since this field modulates the density of states of the electrons at the Fermi-edge. A comparison with Eqn.14 can be used to determine the definition of R_K

$$R_K = \frac{h}{e^2}$$

This is simply the inverse of the conductance quantum, i.e. the conductance of a (spin-split) edge channel. According to Eqn.14, the Hall resistance is a fraction of the factor $R_K I = h/e^2 I$, as long as the current through the probe occurs entirely through the edge channels. The proportionality factor is the number of (spin-split) edge channels, which is equivalently the fill factor ν . The transition between two plateaus in the Hall voltage occurs as magnetic fields where a Landau level overlaps with the Fermi edge. Only in this range can scattering of charge carriers occur, and the Hall voltage (given by $U_H = U_{SD}$) can change continuously. Simultaneously in this magnetic field range the number of edge channels increases by one (or two if spin states are degenerate). The range of magnetic field over which this transition occurs, and therefore also the width of the Hall voltage plateaus, at low temperatures is related to the width of the Landau-levels (Chapter 3.2), or at high temperatures would also be related to the spread of the Fermi-edge, which is on the order of $k_B T$ (Chapter 3.3).

Finally, it should also be noted that without localized states (Chapter 3.2), the one-dimensional edge channels would not exist, and instead the electrons throughout the entire 2DEG would partake in charge transport. The edge channels are essential for quantization of the Hall-effect. Furthermore, because the localization of the electron trajectories only occurs due to disorder and defects in the sample, it would also not be possible to observe the quantum Hall effect in a perfect probe.

The von Klitzing constant h/e^2 can be so precisely defined through the quantum Hall effect measurement, that it is nowadays used worldwide as a resistance standard. Another application of the quantum Hall effect is in determining the fine structure constant α through the relationship

$$\alpha = \frac{e^2}{h} \frac{\mu_0 c}{2} \approx \frac{1}{137} .$$

The von Klitzing constant has been measured to a relative precision of 3×10^{-9} as $R_K = 25812.807449 \Omega$. For more detail regarding the von Klitzing constant, please refer to internet sites of metrology institutes (e.g. PTB: [http:// www.ptb.de](http://www.ptb.de), NIST,...).

4 The Experiment

4.1 Experimental setup and sample properties

The aim of this experiment is to study a two-dimensional electron gas in a GaAs/AlGaAs heterostructure. The sample is located in the lower end of a vacuum tube and in the centre of a superconducting solenoid magnet consisting of NbTi wire. The vacuum tube is filled with a small amount of "exchange gas" in order to have a thermal contact between the sample holder and the liquid helium. The sample is continuously heated by the mounting and the connection wires, therefore the sample is slightly warmer than the 4.2K of the liquid helium bath. Which gas should be chosen as "exchange gas"?

The solenoid magnet is controlled by a power supply. The current may not, under any circumstances, be higher than 25 A! For higher currents the coil will go normal and all of the energy stored in the magnetic field will be released at once. This is called a "quench".

All electrical contacts of the sample are connected with wires. These wires are run to the top of the vacuum tube and connected to BNC connectors. A schematic drawing of the sample is shown in fig.11.

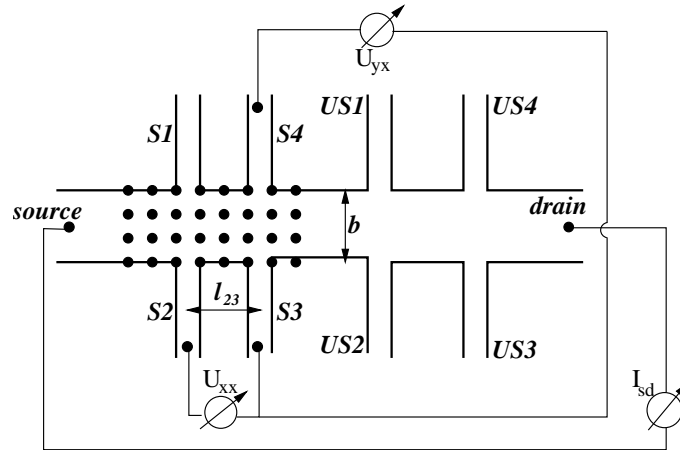


Figure 11: Schematic drawing of the Hall bar.

One part of the sample is unstructured, the other part has an antidot super lattice. Furthermore the sample is coated with a top gate consisting of a 5 nm titanium layer (some samples have an additional, 200 nm thick gold layer). This coating covers the whole surface of the hall bar. A positive or negative voltage applied to the top gate modulates the potential and therefore the charge carrier concentration within the heterostructure. For the data evaluation the relation between the distance of two ohmic contacts (for measuring the longitudinal voltage, see fig.11) and the width of the sample must be known. The sample used in the experiment has a ratio $l_{23}/b \simeq 0.75$.

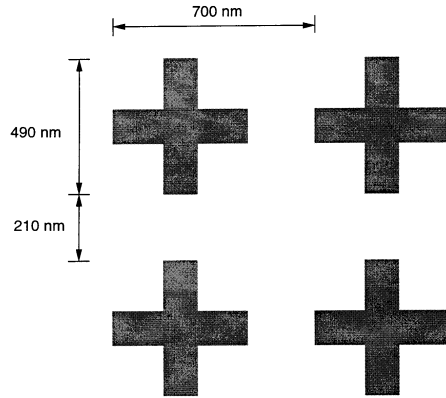


Figure 12: Details of the antidots shown in fig.11 with the dimensions of the cross-shaped antidots *only* applying for samples S1 and S2.

There are several different samples for the experiments. They differ mainly in the dimensions of the antidot super lattice. The samples S1 and S2 have a cross-shaped antidot super lattice (see fig. 12). All other samples have antidots with round, etched holes. In Fig. 13 an AFM (atomic force microscope) image of sample B1 as well as a height profile is shown. In table 1 important parameters of the different samples are listed. Please ask your supervisor, which sample is used in the experiment!

Table 1: important sample parameters

Sample	Form of the antidots	lattice const. of the antidots	Top gate	Top-Gate-Voltages (V)
S1	crosses	700 nm	5 nm Ti	+0.0 +0.5 +1.0
S2	crosses	700 nm	5 nm Ti	+0.0 +0.5 +1.0
B1	round holes	700 nm	5 nm Ti	-0.2 +0.0 +1.0
B2	round holes	840 nm	200 nm Au	-0.65 -0.3 +0.2
D1	round holes	500 nm	200 nm Au	+0.0 +0.2 +0.4
D2	round holes	750 nm	200 nm Au	-0.15 +0.0 +0.5
D3	round holes	500 nm	200 nm Au	-0.2 +0.0 +0.5
D4	round holes	670 nm	200 nm Au	+0.0 +0.25 +0.5

For data evaluation it is necessary to know the current through the sample. In the experiment, a constant voltage (and not a constant current) supply is used. With the help of a series resistor ($1\text{ M}\Omega$) a constant current of $2\text{ }\mu\text{A}$ has to be adjusted. Initially it can be assumed that the sample resistor is much smaller than $1\text{ M}\Omega$ and can be neglected. It must be determined experimentally whether this leads to a systematic error in the current through the sample due to its magnetic field depen-

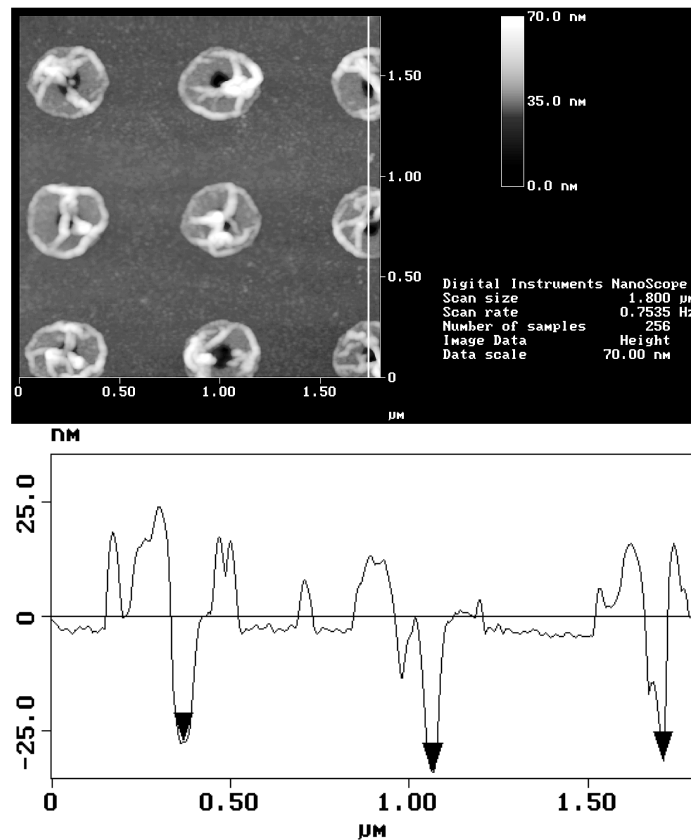


Figure 13: AFM image of the surface (top) of sample B1 and a height profile along the white line in the AFM image (bottom).

dence. All voltages measured in the experiment are amplified with a differential amplifier by a factor of 100.

In fig. 14 a circuit diagram of the experimental setup is given. **The connection of the cables has to be done very carefully! High currents, high voltages or sudden changes in the potential and mechanical shocks can be very harmful to the sample! The source current may not be much higher than $2 \mu\text{A}$, the gate voltage may not exceed the values given in table 1 and no current may be applied to the ohmic side contacts (S1-S4, US1-US4, see fig. 11). Only grounded cables may be connected to the sample!** The voltage can be adjusted with a potentiometer and monitored with a voltmeter.

4.2 Measurement procedure

Before the measurements can be started some preparations have to be made. Your supervisor will help you with these preparations! The vacuum tube has to be evacuated and filled with a few mbar of the exchange gas to ensure a thermal contact between the sample and the liquid helium bath. The vacuum tube and the magnet

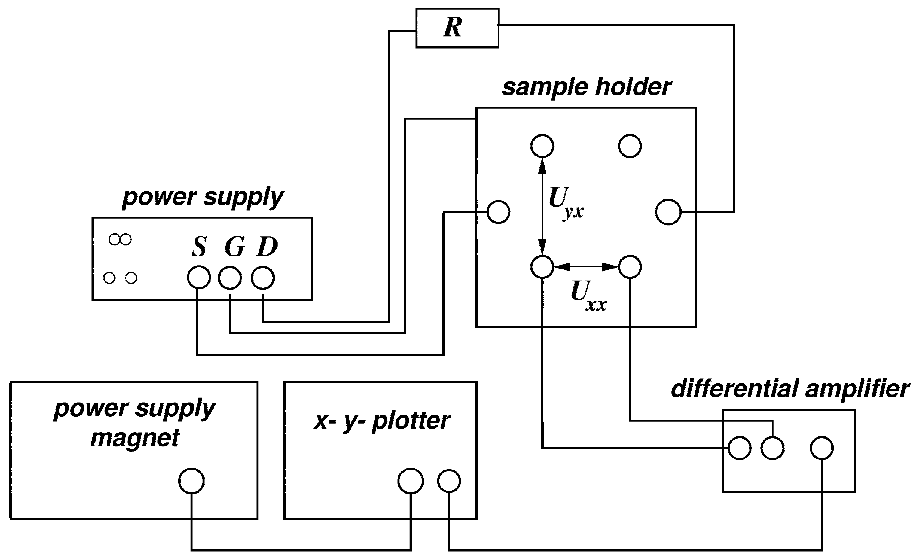


Figure 14: Circuit diagram of the experimental setup.

have to be inserted in the helium can. This must be done very carefully and the pressure in the helium can has to be monitored. If the tube is inserted too quickly, too much of the expansive liquid helium will evaporate due to the very low evaporation heat of Helium (0.0845 kJ/mol). At first the tube should be inserted such that only the surface of the helium bath is touched by the tube. This is accompanied by an increase of the pressure in the can. Then the tube and the sample will be precooled with the gaseous helium which still is very cold. After a while the tube can completely be inserted and the measurements can start.

For each top gate voltage both the longitudinal and the transverse voltage has to be measured for the unstructured part of the sample as well as for the part with the antidot super lattice. Additionally for the unstructured part the classical limits ($B = 0$) have to be measured with high resolution to minimize the error in the evaluation of the mobility. In general the resolution for all measurements should be set as high as possible. Especially the modulations due to the antidot super lattice have to be measured with a high resolution.

The power supply for the magnet is adjusted such that the current is varied automatically from 0 to 25 A and vice versa. Measurements can be done with increasing or decreasing magnetic field. The current through the solenoid can be transformed into a magnetic field with the corresponding coil-dependent constant of proportionality of 0.226 T/A. The voltage output of the power supply delivers a voltage which is proportional to the current with a constant of proportionality of 2.0049 mV/A. This output has to be connected with the input of the x-y plotter.

Finally the error in the assumption of a constant current through the sample has to be determined. Therefore the voltage drop of the whole sample (source-drain voltage) has to be measured. Please note that the serial resistor has to be used

in all causes! (**Caution! Never connect nor disconnect a cable which has an applied voltage! This could damage the sample!**)

For all measurements two big sheets for the x-y-plotter should be enough. It is recommended to use one sheet for the unstructured sample and one for the antidot super lattice. To differ the measurements, different colors can be used. A clear and well defined labeling of each curve is very important!

Enjoy the experiment :-)

4.3 Practical report

The practical report should have a short introduction and a short abstract. The main chapter should include the data analysis, a comparison with theoretical expectations as well as a discussion. Please pay attention to the clear and well-defined labeling of the measured curves.

1. Unstructured and structured areas:
 - (a) Evaluate the most profound statistic and systematic sources of errors and estimate them as realistically as possible. Please estimate quantitatively the error in the assumption of a constant current with the help of the source-drain voltage measurement. Use these error estimations for all further evaluations.
 - (b) Determine the charge carrier concentration from the slope of the hall voltage. Draw the classical Hall line over the whole measurement curve to minimize read out inaccuracies. Does the measured curve match your expectations?
 - (c) Determine the plateau values of the hall resistance and its corresponding filling factors. Avoid employing the literature value of the von-Klitzing constant.
 - (d) Do the calculated filling factors match your expectations? Which measured quantities contribute to the values of the filling factors in (16), if the literature value of the von-Klitzing constant is assumed to be known? Do you suspect a systematic error for one of the measured quantities? Can it be quantified?
 - (e) Determine the charge carrier concentration from the Shubnikov-de-Haas oscillations. For this the filling factors of the SdH minima and the SdH maxima have to be plotted as function of the reciprocal magnetic field ($1/B$). Which curve behavior would you expect? Hint: In some samples additional SdH oscillations can occur due to a parallel two-dimensional conducting layer with a different charge carrier density.

- (f) Determine the electron mobility from the longitudinal voltage U_{xx} at $B = 0$.
 - (g) Plot the charge carrier concentrations as well as the mobilities as functions of the top gate voltage. Are the charge carrier concentrations determined by the different methods in agreement within the experimental error? Compare and interpret your results. Try to explain the dependence of the mobility on the charge carrier concentration. Discuss your results for the different parts of the sample (with and without the antidot super lattice).
 - (h) Compare the results of the different methods and the results of the different parts of the sample. Are the results in agreement with your expectations?
2. Only for the structured part:
- (a) Interpret the maxima in the longitudinal voltage, which cannot be explained with SdH oscillations.
 - (b) Identify possible trajectories in the antidot lattice. (Drawing!)
 - (c) For which magnetic field are runaway trajectories dominant? Compare your expectations with the experiment.
 - (d) Explain qualitatively the observed dependence of the top gate voltage on the electron trajectories. Can you make a statement about the antidot potential? (Hint: Consider the dependence of the top gate voltage on the Fermi energy)

5 Further Reading

1. K.Kopitzki, "Einführung in die Festkörperphysik", Teubner Studienbücher
2. H.Ibach/H.Lüth: "Festkörperphysik. Einführung in die Grundlagen", Springer Verlag
3. J. Singleton u.a., "Band Theory and Electronic Properties of Solids", Oxford University Press
4. S. Datta, "Electronic Transport in Mesoscopic Systems", Cambridge University Press
5. M. Janßen, O. Viehweger, U. Fastenrath, J. Hajdu, "Introduction to the Theory of the Integer Quantum Hall Effect", VCH Verlagsgesellschaft
6. Originalarbeit von Klaus von Klitzing: K. von Klitzing, PRL 45, 494 (1980)
7. Vortrag anlässlich der Nobelpreisverleihung: K. von Klitzing, Reviews Of Modern Physics 58, 519 (1986) bzw. <http://www.nobel.se>

English translation:
Sarah Wittig, 12/2014